Mask roughness induced LER: a rule of thumb

Brittany M. McClinton[1] and Patrick P. Naulleau[2]

[1] Dept. of Electrical Engineering, University of California, Berkeley, CA 94720
[2] Center for X-Ray Optics, Lawrence Berkeley National Laboratory, Berkeley, CA 94720

ABSTRACT

Much work has already been done on how both the resist and line-edge roughness (LER) on the mask affect the final printed LER. What is poorly understood, however, is the extent to which system-level effects such as mask surface roughness, illumination conditions, and defocus couple to speckle at the image plane, and currently factor into LER limits. Here, we propose a "rule-of-thumb" simplified solution that provides a fast and powerful method to obtain mask roughness induced LER. We present modeling data on an older generation mask with a roughness of 230 pm as well as the ultimate target roughness of 50 pm. Moreover, we consider feature sizes of 50 nm and 22 nm, and show that as a function of correlation length, the LER peaks at the condition that the correlation length is approximately equal to the resolution of the imaging optic.

Keywords: extreme ultraviolet, lithography, LER, mask roughness, speckle

1. INTRODUCTION

As extreme-ultraviolet lithography (EUVL) moves towards commercialization and pushes to ever smaller critical dimensions (CDs), achieving the stringent requirements for line-edge roughness (LER) is increasingly challenging. For the 22-nm half-pitch node, the International Roadmap for Semiconductors [1] calls for less than 1.2 nm LER. Currently, state-of-the-art EUVL tools can consistently achieve only about 3 nm LER. It is apparent that in order to reach the industry's goal, further progress needs to be made in understanding the principle causes of LER. Moreover, it would be beneficial to develop analytic solutions for fast feedback.

Traditionally, LER has been viewed as a resist-limited effect. As CDs shrink, however, mask contributors become more and more important. For EUVL in particular, three major contributors (resist LER, mask LER, and mask roughness induced LER) must be taken into account. Much research has already been done to develop analytic tools to predict resist LER [2]. Other studies have examined analytically how the LER on the mask couples to the printed LER [3]. While significant work has been made in understanding how mask roughness couples to speckle in the aerial image and hence to LER [4-9], the extent to which it currently factors into LER limits remains incompletely understood. Moreover, there is no method known to the authors to easily calculate its contribution, given illumination conditions and defocus. Rather, to predict mask roughness induced LER, one needs to conduct full 2D aerial image simulations in one software package and then extract the LER in another. This method is time consuming and cumbersome. Here, we propose a tractable simplified solution to mask roughness induced LER to expedite research and understanding.

2. MASK ROUGHNESS INDUCED LER – A PROBLEM

Before investigating possible simplified methods to predict mask roughness induced LER, it is important to understand how it arises. As discussed in the literature [4,7,10] and therefore only briefly presented here, surface roughness on a reflective mask geometrically induces phase roughness on the wavefront that due to the reflection is a factor of two larger than the actual surface deviations. This effect has detrimental consequences for EUVL. Since the operating wavelength is nominally 13.5 nm, very small roughness on the multi-layer mask can significantly modulate the phase. While the lithographic process operates by reimaging the mask to the wafer, the process itself is band-limited, resulting in an imperfect replication of the mask object that is sensitive to the phase errors on it. Phase roughness on the mask results in many overlapping amplitude spread functions in the image plane that differ in phase from one to another,

causing a complex interference pattern, the strength of which is modulated by the coherence factor. These interference events manifest themselves as intensity variations, or speckle, at scales down to the resolution limit of the objective [11].

It is apparent that speckle is a complex phenomenon. However, it is a statistical effect whose macroscopic properties can be largely described by specifying the objective NA, coherence factor σ, defocus, and, of course, mask roughness.

Although it is not impossible to describe a mask completely by every detail of its surface roughness, it is more useful to describe it in terms of its macroscopic properties. By doing so, its speckle statistics are shared by a much wider set of masks, all differing in microscopic detail, but sharing these macroscopic properties.

In order to elucidate the macroscopic properties of importance, let us picture roughness as random "bumps" covering the surface of the mask. We assume these bumps to be replicated through the various layers comprising the multilayer thus truly effecting the phase of the reflected beam. We refer to this roughness as replicated surface roughness (RSR). The other property of concern is the extent to which the bumps are laterally self-similar on the mask. This property is characterized by the correlation length. It is a measure of the extent to which the roughness is dephased laterally across the wavefront with respect to itself, and it governs the spatial frequency content of the roughness on the mask. Thus, for example, greater height variations (RSR) and lesser self-similarity across the mask (correlation length) mean that the mask is "rougher" in a statistical sense.

By expressing mask roughness in terms of correlation length and RSR, its macroscopic roughness properties are well determined. When combined with the parameters of the objective NA, coherence factor σ, and defocus, the speckle statistics can then theoretically be determined (see Fig. 1). We express this speckle as *S*. Although analytic solutions for the clear-field speckle are certainly feasible, dealing with system parameters such as aberrations (including defocus) considerably complicate the issue. Thus, the more practical approach is to use modeling to predict the speckle.

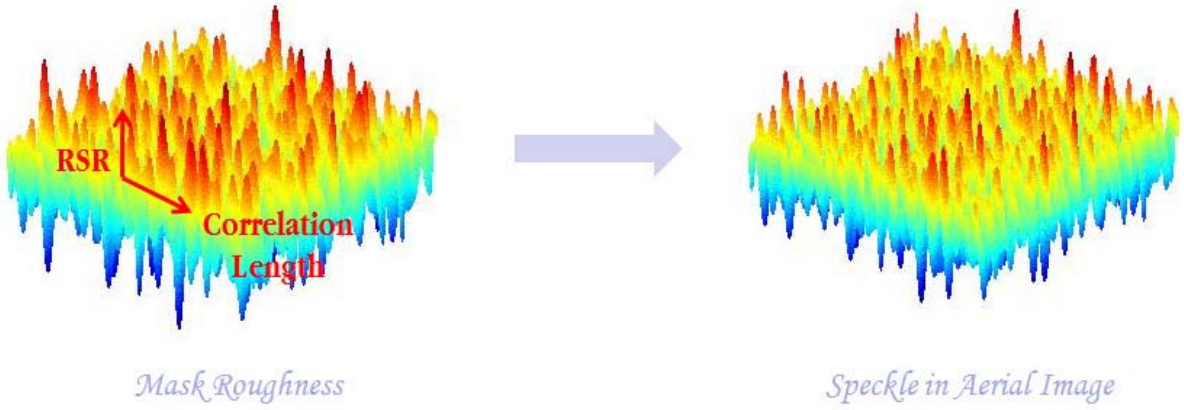

Fig. 1. Mask roughness statistics combined with illumination and band-limited imaging well determines speckle statistics in the aerial image.

Ultimately of interest, however, is the LER and not the speckle. The strength of how the speckle couples to LER is determined by the image-log-slope (ILS). Typically used as a metric of image quality, it measures the slope of the aerial image intensity transition across the edge of features present on a mask; e.g. from line to space. Essentially, it is the change in intensity over change in position across the edge. By definition, it is

$$ILS = \frac{d\ln I}{dx} = \frac{1}{I}\frac{dI}{dx} \qquad (1)$$

where the intensity, *I*, is the threshold at which the ILS is evaluated. It is dependent on the objective NA, coherence factor σ, CD, and defocus. A higher ILS means that for any intensity variation (e.g., through speckle), the resulting

change in line-edge position will be small in comparison to a lower ILS value. Therefore, a higher ILS is desirable, from the perspective of minimizing sensitivity to mask roughness.

Noting that movements in line-edge, *dx*, are directly related to the 3-sigma definition of line-edge roughness, we can formalize the relation between speckle statistics and LER as

$$LER = 3 \times dx = 3 \times S \times \frac{1}{Intensity \times ILS}. \quad (2)$$

3. MASK ROUGHNESS INDUCED LER – AN ANALYTIC SOLUTION

Current methods to predict mask roughness induced LER involve conducting full 2D aerial image simulations in commercially available software (such as PROLITH [12] or Panoramic [13]), followed by extracting the LER from the computed aerial image through offline analysis using a software package such as SuMMIT [14]. As stated earlier, this method is time consuming and cumbersome.

Our goal instead, is to simplify the LER modeling process by using simplified form of Eq. 2. The power in this simple equation is not in any new formulation, but in the method of implementing it. By looking at Eq. 2, we can break-up the problem into smaller parts. Consider an imaging system of given objective NA. Instead of doing 2D aerial image simulations for each process parameter individually, we can minimize this time-consuming process by only conducting a one-time 2D aerial image simulation through focus on a clear-field rough mask to get the illumination- and mask roughness-specific clear-field speckle. We can then couple this speckle to LER by using fast 1D aerial image simulations (e.g., using PROLITH) to get the feature- and illumination-specific ILS as it varies through focus. From here, the full parameter space can be reached by analytic extension. A comparison schematic of the two methods is shown in Fig. 2.

There are two distinct advantages to such a formulation. Firstly, it provides a straightforward, tractable simplified solution to computing mask-roughness-induced LER that is fast. Secondly, there is no need for an exhaustive list of 2D aerial image simulations for every mask pattern to be considered.

4. MODELING APPROACH

To verify the validity of our approach, we need to compute the LER from both methods illustrated in Fig. 2 and compare them. Both used scalar aerial image modeling software based on the equations of partially coherent image formation [11]. Commercial software with similar capabilities include PROLITH [12] and Panoramic [13]. We modeled an aberration-free optical system with NA = 0.32. Again, the low NA allows for scalar and thin mask modeling. Following a similar numerical analysis approach used elsewhere [7], we constructed a statistical representation of a clear rough mask as a random phase object, whose pure phase distribution is determined from the geometric path length differences imparted by the rough surface of the mask. We started with a randomly generated mask object that was 1024 x 1024 pixels at 1 nm / pixel with 1:1 imaging to the wafer plane. The standard deviation of the original height map of the mask object was calculated to verify the RSR value. By taking the FWHM of the autocorrelation of the mask, the correlation length was found. Using this process we generated an entire set of masks all with an RSR of 50 pm, and with a variety of correlation lengths (5, 13, 20, 26, 32, 42, 47, 61, 68, 83, 96, 106, 127 nm). In order to build up a significant statistical ensemble, we created 10 random realizations of the mask for each RSR / correlation length pair. Assuming a wavelength of 13.5 nm, we converted each topographic surface to a phase perturbation. This set of masks was the starting point for the two approaches we wish to compare: the traditional method and the proposed simplified one.

To reproduce the traditional method which calls for calculating the LER directly from aerial-image simulations, we overlaid (multiplied) each clear-field rough mask realization with an ideal binary amplitude 50 nm line-space pattern.

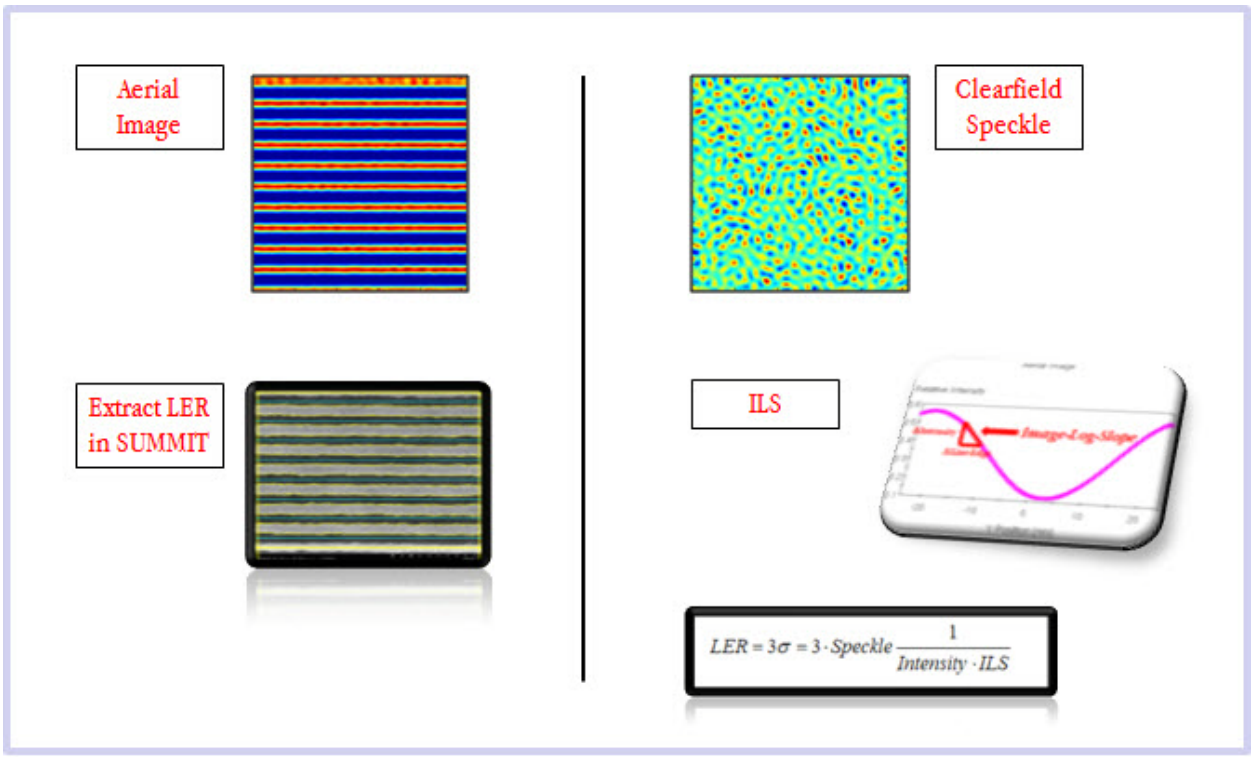

Fig. 2. A comparison schematic of the traditional method and the simplified method to get the mask roughness induced LER.

We carried out the simulations through focus for 4 different disk illuminations: coherence factors σ = 0.15, 0.25, 0.50, and 0.75. We then extracted the LER in SuMMIT [14], using only nested features for LER analysis, avoiding the outer 200 nm border. We took care to set the binary threshold properly for each sigma value to provide proper sizing of the 50 nm lines at best focus. This was done for each random realization of each mask to build up the statistics. Assuming the process is ergodic, we could have just as easily used a larger mask with larger lengths of lines instead of numerous independent realizations. However, due to memory constraints, our chosen method is the preferred one. The LER data from this traditional approach is now ready for comparison to the new simplified method.

For the simplified method, we modeled each random realization of the clear-field mask under the same illumination conditions to get the clear-field speckle statistics. We then calculated the ILS using fast 1D aerial-image simulations in PROLITH [12] for our pattern of lines and spaces for each illumination condition. Finally, using the proposed solution to mask roughness induced LER described above, we analytically calculated the LER.

It is important to note that the power of the simplified approach lies in the one-time intensive aerial-image simulations of the clear-field speckle statistics. Once calculated, they are done. By using feature-specific ILS to couple clear-field speckle to LER in the aerial image, we can analytically extend the LER analysis to an arbitrary set of features with great ease.

5. VERIFICATION OF THE SIMPLIFIED MODEL

Fig. 3 shows simulated LER results for one illumination setting, σ = 0.15. The trends for each correlation length show fairly constant slopes through focus with no crossover between them. This pattern is consistent for all other illuminations as well. It is therefore possible, for clarity, to look at just one defocus setting for comparison of the simulated LER to the simplified approach.

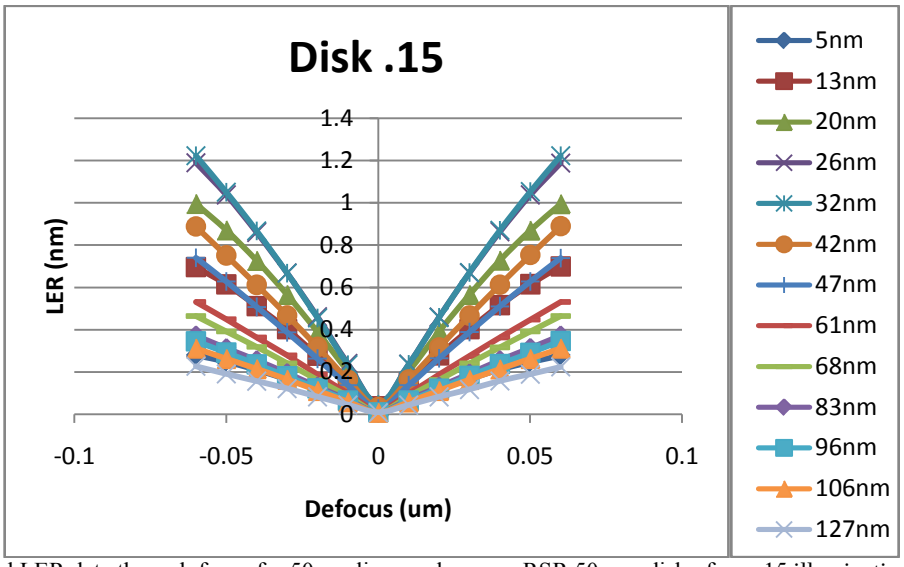

Fig. 3. Simulated LER data through focus for 50 nm lines and spaces, RSR 50 pm, disk of σ = .15 illumination, for a variety of correlation lengths.

Our first attempt to verify the simplified method against the full calculation did not provide a good match (see Fig. 4). This suggests that the clear-field speckle differs significantly from the speckle in the presence of lines and spaces. To assert this, we directly compared the intensity standard deviation of the clear-field aerial image and that of the feature-specific one (taken both at the line-edge and in the middle of the space). In this calculation, we used the aerial image results from the simulated LER method to investigate the feature-specific speckle. We took the standard deviation of the intensity in the direction parallel to the lines at two horizontal positions: in the middle of the space and at the line-edge (see Fig. 5 for a comparison of the two methods). We also took care to evaluate the line-edge intensity standard deviation at the same threshold value used for calculating the simulated LER. The results show great disparity (see Fig. 6). It is apparent that the presence of features affects speckle in a complex way.

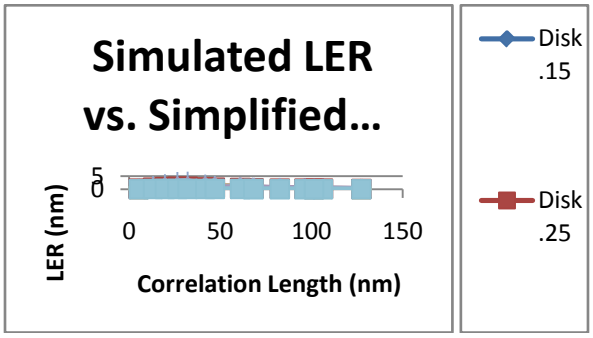

Fig. 4. Our first attempt provided a poor match. Simulated LER vs. Simplified LER (using clear-field speckle) at -50 nm defocus setting for a variety of correlation lengths and a variety of illumination settings.

Therefore, in its most general form, the simplified method must use the speckle at the line-edge. To prove its validity, we attempted the comparison between the full calculation and simplified method once again, but this time using the standard-deviation of intensity at the line-edge. The results are shown in Fig. 7 (top-left) are at a defocus setting of -50 nm and give an excellent match. We repeated the entire data set for 40 nm lines and spaces and 22 nm lines and spaces, the results of which are shown in Fig. 7. We also repeated the entire data set on 50 nm and 22 nm lines and spaces for a different RSR value of 230 pm, shown in Fig. 8. For Fig. 8 at 22 nm lines and spaces, the defocus setting was changed slightly to -30 nm, due to corrupted image files further out of focus. In all cases, there was good agreement between the full and simplified LER methods. In Fig. 8 for 22 nm lines and spaces at 230 pm RSR, the match between the two methods agrees less well for higher correlation lengths, but we believe this is a simple artifact of the statistical nature of the speckle. Since the line-edge speckle calculation used only one line-edge on one aerial image, this could likely be improved by considering a larger dataset.

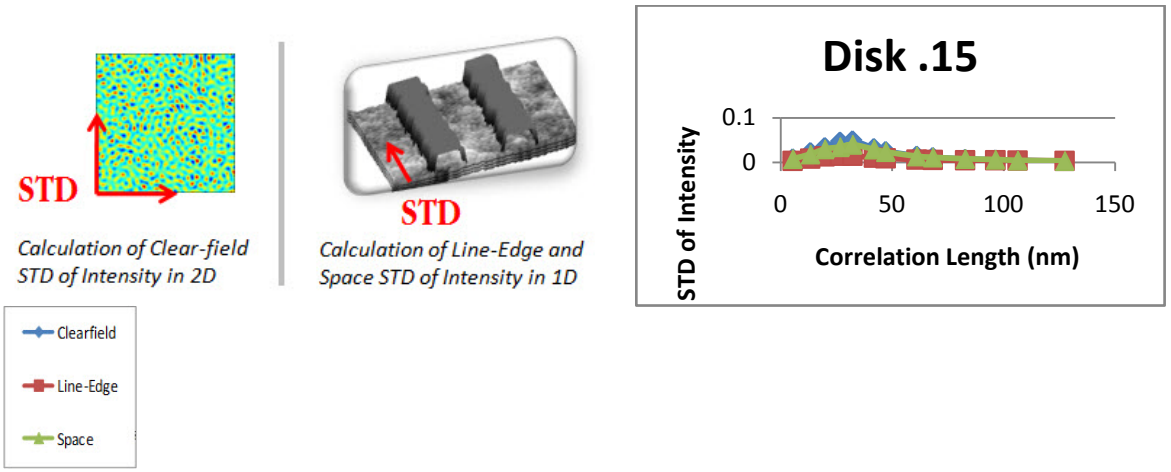

Fig. 5. (Left) Clear-field speckle vs. Line-edge speckle calculation method.
Fig. 6. (Right) STD of Intensity of Clear-field vs. at the Line-edge and middle of the Space for 50 nm lines and spaces with disk illuminations σ = .15, RSR 50 pm, for a variety of correlation lengths at -50 nm defocus.

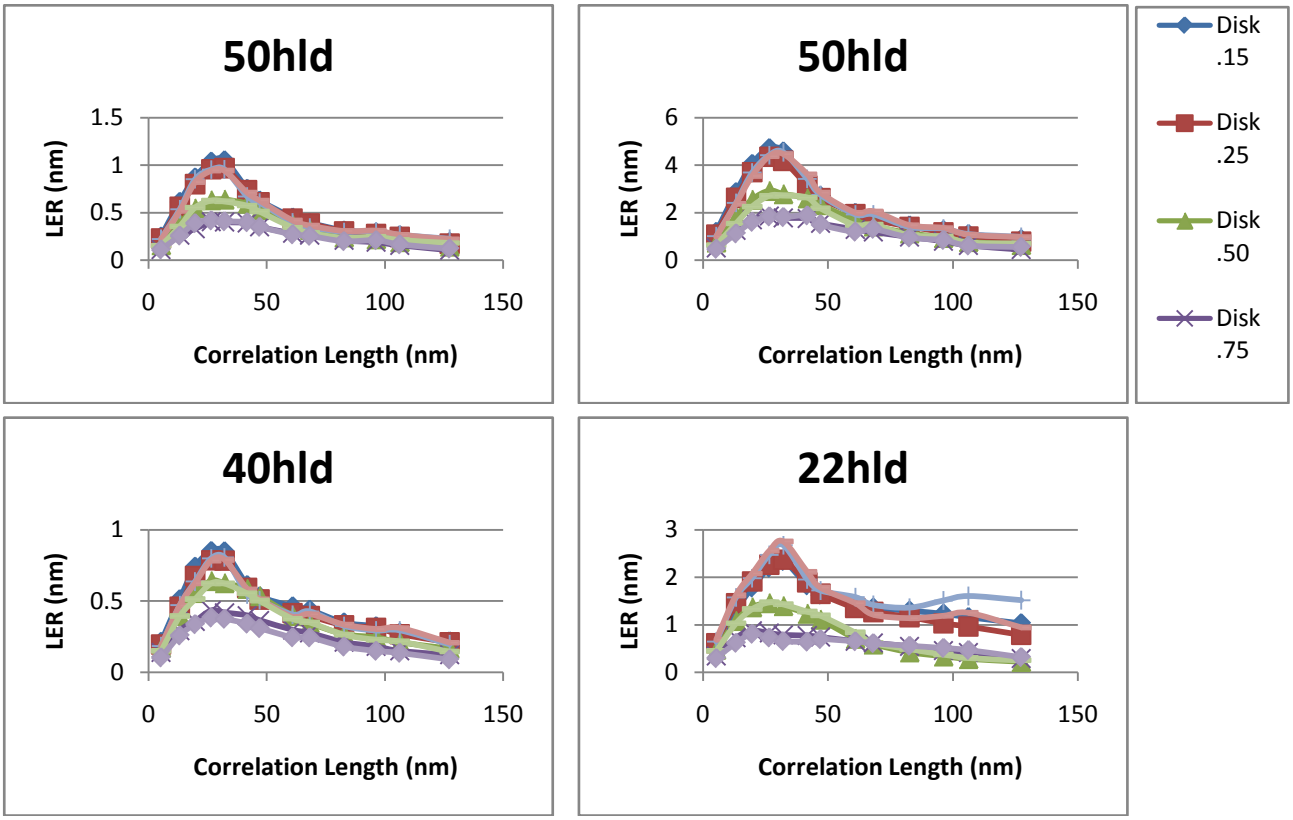

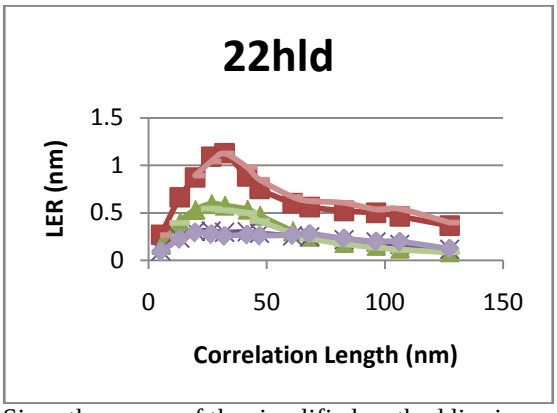

Fig. 7. Simulated LER vs. Simplified LER (using speckle at Line-edge) for RSR 50 pm, a variety of illuminations, a variety of correlation lengths, at a defocus of -50 nm, for (top-left) 50 nm, (center-left) 40 nm, and (bottom-left) 22 nm lines and spaces.

Fig. 8. Simulated LER vs. Simplified LER (using speckle at Line-edge) for RSR 230 pm, a variety of illuminations, a variety of correlation lengths, (top-right) at a defocus of -50 nm for 50 nm lines and spaces, and (bottom-right) at a defocus of -30 nm for 22 nm lines and spaces.

Since the power of the simplified method lies in applying the clear-field speckle formulation and *not* the line-edge one, we investigated how to functionally relate the one to the other. If we found some way to do so, then we could maintain the clear-field speckle formulation with perhaps some adjustment parameter. Assuming the relative intensity variation in the case with lines to be constant and equal to the relative variation in the clear-field speckle, we can approximate the absolute intensity variation (speckle) at the edge to be the absolute clear-field speckle scaled by the relative intensity at the edge. Thus, if the edge is defined at a threshold value of 30%, for example, we would assume the absolute speckle at the edge to be 30% of the absolute speckle in the clear-field. To test this assumption, we constructed a knife-edge structure on top of a clear-field rough mask of RSR 50 pm, using one of the previously generated realizations of the clear rough mask for the 32 nm correlation length case (see Fig. 9). We carried out aerial image simulations for the same 4 disk illuminations examined above, and extracted the resulting LER. We then calculated the clear-field speckle and the ILS, in a similar manner to that described above, and repeated the calculation of LER using the clear-field speckle as in Eq. 2, but where the clear-field speckle was scaled by the line-edge intensity (found in PROLITH[12]). The numerical results are seen in Fig. 10, and show that the scaled clear-field speckle formulation actually provides a better agreement with the simulated LER values than does the simulated line-edge speckle formulation, for the case of the knife-edge. We believe this is because the standard deviation of the line-edge captures not only the line-edge speckle, but deviations caused by the LER itself as well, resulting in a overestimation of the LER.

We then repeated the comparison between simulated LER and the LER calculated from the simplified model, shown in Fig. 7 (top-left). This time, however, we used the new scaled clear-field speckle for the simplified model. The results shown in Fig. 11 show a good match. The simplified model seems to consistently underestimate the simulated LER by only a small amount for all illuminations, approximately 0.1 nm at most.

Disk Illumination	σ =0.15	σ = 0.25	σ = 0.50	σ = 0.75
Clear-field Speckle	0.0493	0.0444	0.0256	0.0129
ILS	92.3	90.7	83.6	72.5
Intensity at line-edge	0.272	0.266	0.284	0.305
LER from Simplified Model	**1.45**	**1.3**	**0.87**	**0.54**
Simulated LER	**1.2**	**1.1**	**0.7**	**0.4**

Fig. 9. (Left) Knife-Edge on rough clear mask with RSR 50 pm and correlation length of 32nm.
Fig. 10. (Right) Numerical results for the calculation of LER based on the simplified model in comparison with the LER calculated from the full 2D aerial image simulation.

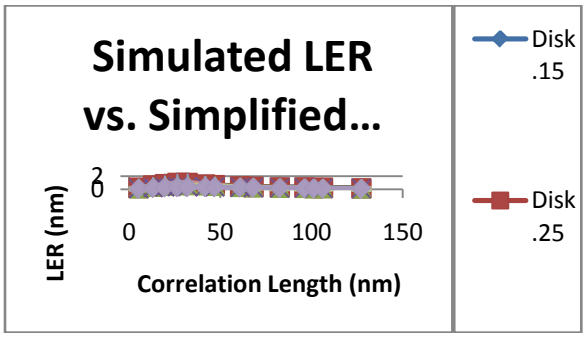

Fig. 11. When the clear-field speckle is scaled by intensity at the line edge, the LER based on the simplified model matches the simulated LER well. For all illuminations, the LER is consistently underestimated by only a small amount, approximately 0.1 nm at most. This is for 50 nm lines and spaces with an RSR 50pm at a defocus of -50nm, for a variety of correlation lengths and illumination settings.

6. DISCUSSION

A simplified solution exists for predicting mask roughness induced LER.

The power of the simplified solution lies in being able to use the clear-field speckle formulation, where there is no need to repeat intensive 2D aerial image simulations for each specific feature. A one-time clear-field rough mask simulation for the illumination of interest will suffice, scaled by the intensity at the line-edge, with fast 1D aerial image simulations of the ILS to couple LER to any specific feature desired. This clear-field speckle formulation of the simplified solution provides a fast and tractable means of quickly calculating the mask roughness induced LER.

In the course of data accumulated here, all simulations conclusively show that the LER peaks for mid-spatial frequency roughnesses (26nm, wafer dim.), about the resolution of our optic (from the Rayleigh resolution of 0.62λ /NA). This confirms earlier findings [5] that this peak seems to be related to the resolution of the imaging system. In our case, however, it disproves the simultaneous claim [5] that it is likely object dependent, since we observed the peak in the same location for all three feature sizes we investigated: 50, 40, and 22 nm lines and spaces.

The decrease in LER for smaller correlation lengths we believe arises from high spatial frequencies of the scattering halo surrounding the diffracted orders falling out of the pupil. In this way, the objective lens provides a filtering benefit: assuming a fixed RSR, it is equivalent to saying the spatial roughness is decreasing as greater scattering from smaller correlation lengths throws increasingly more light out of the pupil. To the extent that this high frequency content is constant across the field, one would expect the roughness-induced reflectivity loss and thus the intensity modulation to also be constant limiting its impact on LER. On the other side of the LER peak where the correlation length is greater than the resolution of the optic, the LER falls again gradually. Here, all the light is captured by the pupil; this adverse effect, however, is mitigated due to a decreasing rate of change of the induced phase roughness.

As is apparent from Figs. 7 and 8, achieving an RSR of approximately 50 pm will be required in order to push down the mask roughness induced LER contribution to below 1 nm. This is necessary if the total combined LER (due to resist LER, LER on the mask, and mask roughness induced LER) is to be under the 1.2 nm goal for the 22 nm half-pitch fabrication node [1]. Moreover, mid-spatial frequency roughnesses near the resolution limit of the optic should be avoided. In anticipation of the movement towards high NA EUVL tools, future work will extend these simulations to higher NA.

7. ACKNOWLEDGEMENTS

The authors are grateful for the support of this work by the National Science Foundation EUV Science and Technology Center. This research was also supported in part by SEMATECH and carried out at Lawrence Berkeley National Laboratory's Advanced Light Source, which is supported by the Director, Office of Science, Office of Basic Energy Sciences, of the U.S. Department of Energy under Contract No. DE-AC02-05CH11231.

REFERENCES

1. International Technology Roadmap for Semiconductors, 2009 ed., http://public.itrs.net/.

2. G. Gallatin, "Resist Blur and Line Edge Roughness," Proc. SPIE **5754**, 38-52 (2005).

3. P. Naulleau and G. Gallatin, "Line-edge roughness transfer function and its application to determining mask effects in EUV resist characterization," Appl. Opt. **42**, 3390-3397 (2003).

4. T. Milster and N. Beaudry, "Scattering and Coherence in EUVL," in *Emerging Lithographic Technologies II*, Y. Vladimirsky, ed., Proc. SPIE **3331**, 537-543 (1998).

5. N. Beaudry and T. Milster, "Effects of mask roughness and condenser scattering in EUVL systems," in *Emerging Lithographic Technologies III*, Y. Vladimirsky, ed., Proc. SPIE **3676**, 653-662 (1999).

6. N. Beaudry and T. Milster, "Effects of object roughness on partially coherent image formation," Opt. Lett. **25**, 454-456 (2000).

7. P. Naulleau, "Relevance of mask-roughness-induced printed line-edge roughness in recent and future extreme-ultraviolet lithography tests," Appl. Opt. **43**, 4025-4032 (2004).

8. P. Naulleau and G. Gallatin, "Spatial scaling metrics of mask-induced line-edge roughness," J. Vac. Sci. Technol. B **26**, 1903-1910 (2008).

9. P. Naulleau, D. Niakoula, and G. Zhang, "System-level line-edge roughness limits in extreme ultraviolet lithography," J. Vac. Sci. Technol. B **26**, 1289-1293 (2008).

10. P. Naulleau and S. George, "Implications of image plane line-edge roughness requirements on extreme ultraviolet mask specifications," Proc. SPIE **7379**, 1-11 (2009).

11. J. W. Goodman, *Statistical Optics* (Wiley, New York, 1985), Chap. 7, pp. 286-360.

12. PROLITH is a registered trademark of KLA-Tencor Corporation, 160 Rio Robles, San Jose, Calif. 95134.

13. Panoramic Technology, Inc., "Em-suite: core lithography simulation package," (2009), see http://www.panoramictech.com.

14. SuMMIT.